J. Chem. Sci. Vol. 129, No. 2, February 2017, pp. 157–166. © Indian Academy of Sciences.
DOI 10.1007/s12039-016-1212-z

REGULAR ARTICLE

In situ grown nano-architectures of Co_3O_4 on Ni-foam for charge storage application

G RAJESHKHANNA, EDIGA UMESHBABU and G RANGA RAO*
Department of Chemistry, Indian Institute of Technology Madras, Chennai, Tamil Nadu 600 036, India
Email: grrao@iitm.ac.in

MS received 15 October 2016; revised 19 November 2016; accepted 27 November 2016

Abstract. Nanostructured Co_3O_4 on Ni-foam has been synthesized with diverse morphologies, high surface area and porosity by employing different surfactants under hydrothermal conditions and subsequent calcination. The surfactants strongly influence the physicochemical properties of cobalt oxide samples. The cobalt oxide grown on Ni-foam without surfactant had flower-like morphology. However, cobalt oxides synthesized by using cationic (CTAB) and non-ionic (Triton X-100) surfactants showed flake-like morphology, but the spatial arrangement of flakes was found to be different in both the samples. The surfactant-assisted cobalt oxide showed average crystallite size of ~6.6–9.8 nm, surface area of 60–80 m^2g^{-1} and porosity (pore diameter ~3.8 nm). These samples were found to perform better as charge storage electrode materials. The specific capacitance values of cationic and non-ionic surfactant-assisted cobalt oxide materials, at a current density of 1.0 A g^{-1}, were 1820 and 806 F g^{-1}, respectively, compared to 288 F g^{-1} of cobalt oxide prepared without surfactant. They also showed excellent capacity retention for over 3000 charge-discharge cycles at higher current densities. The difference in the capacitance values of cationic and non-ionic surfactant-assisted cobalt oxide is due to the difference in the flake arrangement.

Keywords. Nano-architecture; Ni-foam; Co_3O_4; charge storage.

1. Introduction

To date, extensive progress has been made in the preparation of a variety of nanostructured materials using solution-based methods. Among the various nanostructured materials metal oxides have great potential to satisfy many requirements in diverse application fields because of the availability of multiplicity of structures, high thermal stability and controllable morphological features. Over the past several years, metal oxides and carbon materials have been tremendously exploited particularly in electrochemical energy storage and conversion, and in non-electrochemical processes.[1–11] Oxides are particularly important because of the variable oxidation states of metal ions and stable structures. Cobalt oxide is one of the best oxide materials and has been recognized as a propitious electro-active electrode material in supercapacitors,[10–17] sensors,[13,17,18] batteries[2,4,19] and electrocatalysis[20–22] owing to better reversibility and environment-friendly nature. Cobalt oxide exists in three forms such as cobalt (II) oxide (cobaltous oxide, CoO), cobalt (III) oxide (cobaltic oxide, Co_2O_3) and cobalt (II, III) oxide (cobaltosic oxide, Co_3O_4). Among these, spinel Co_3O_4 has a more stable structure, catalytically more active and easier to synthesize, and therefore it is most widely studied for electrochemical applications.[2,10–21,23] In recent years, by employing solution based methods Co_3O_4 have been synthesized in miscellaneous morphologies and different sizes.[2,10–21,23] These faceted morphologies include nanowires,[10] ultralayered 2D sheets,[11] and ultrathin nanosheets,[12,13,15] microspheres,[16] nanoboxes[23] and many more.[2] It is important to point out that the performance of Co_3O_4 in energy related applications, especially in supercapacitors and electrocatalysis, depends primarily on the crystalline structure and surface properties.[2,5–17,20,21] In this context, we focused on tailoring of Co_3O_4 material with well-defined properties and favourable morphologies for supercapacitor application.

Supercapacitors are promising high power energy storage devices in which metal oxides and carbon based materials are widely used as the electrode material; carbon materials store energy by non-Faradaic process while metal oxides store energy by Faradaic process in which reversible redox reactions can occur rapidly.[1,6,10–17,24,25] In this perspective, spinel Co_3O_4 exhibits better reversibility and higher theoretical capacitance value of 3560 F g^{-1}. Hence, spinel Co_3O_4 is a prominent material to use as an electrode

*For correspondence

material in supercapacitors.[12,14,15] Many attempts have been reported in the literature to improve the specific capacitance value of spinel Co_3O_4 with good cyclic stability.[10–17] Table S1 (in Supplementary Information) shows the comparison of specific capacitance values (C_S) and capacity retention of recently reported Co_3O_4 materials. In literature, only a few reports have shown higher C_S and good cyclic stability for Co_3O_4 material. In many cases, the common reason for low C_S value and poor capacitance retention is attributable to limited utilization of electrode material during charge-discharge processes. The binder poly(vinylidenedifluoride) (PVdF) commonly used to fabricate the electrode material blocks electroactive sites, and fades the conductivity. These factors are detrimental to supercapacitor performance.[15] In addition, charge storage performance of the oxide material obliquely depends on crystalline structure, exposed facets, surface area, pore distribution, morphology, electrical conductivity and nature of current collectors.[2,10–17,26–29] Therefore, it is necessary to employ diverse synthetic and fabrication strategies to achieve the best possible electrode materials with controlled size, shape and other desirable physicochemical properties. Hydrothermal process is a prominent and widely employed method to synthesize energy storage materials.[2–14,26–30] This is an expedient method to deposit *in situ* the electro-active material on current collector such as Ni-foam without adding binders during the fabrication of electrodes.[12–14,27,28,30,31] The electrode material grown *in situ* on Ni-foam can exhibit good electrical conductivity, low diffusion resistance and high electro-active surface area.[15,31]

Nevertheless, to meet the higher requirements of future systems, we need to develop a Co_3O_4 material to further enhance its specific capacitance. Here, we report a lucrative and simple strategy to grow spinel Co_3O_4 precursors directly on Ni-foam and subsequent calcination to fabricate binder-free oxide electrode for high-performance electrochemical energy storage application. We have adopted simple hydrothermal homogeneous precipitation method with hexamethylenetetramine as precipitating agent. Cationic and non-ionic surfactants have been employed in order to tune the morphology, to increase surface area and porosity. All these properties will in turn play vital role in improving the supercapacitor performance. We demonstrated systematic comparison of physicochemical and electrochemical properties of spinel cobalt oxide grown on Ni-foam mediated by surfactants. We report that cetyltrimethylammonium bromide (CTAB)-initiated cobalt oxide ultrathin nanoflake arrays grown on Ni-foam exhibit high specific capacitance value of 1820 F g^{-1} at current density of 1 A g^{-1}. The 4-octylphenol polyethoxylate (Triton X-100)-initiated spinel cobalt oxide ultrathin nanoflake arrays grown on Ni-foam showed excellent cyclic stability of 116% specific capacitance retention even after 3000 cycles at a current density of 8 A g^{-1}.

2. Experimental

2.1 *Fabrication of nanostructured Co_3O_4 on Ni-foam*

In this experiment, 1.2 mmol of $Co(NO_3)_2{\cdot}6H_2O$ and 2.4 mmol of NH_4F were dissolved in 30 mL of triple distilled water and stirred for 1 h to form a homogeneous pink solution. 1.2 mmol of solid hexamethylenetetramine was added to the resulting solution and continued stirring for 2 h to attain complete homogeneity. Ni-foam (approximately 1 cm × 1 cm) was carefully cleaned with HCl solution (3 M), sonicated in triple distilled water and finally with acetone in an ultrasonic bath to remove surface NiO layer. The cleaned Ni-foam was used to deposit cobalt oxide material under hydrothermal conditions. The aqueous salt solution and Ni-foam were transferred to a Teflon lined autoclave of 50 mL capacity and subjected to heating at 120°C for 12 h. Under these conditions, the solid material was deposited uniformly on the clean Ni-foam. The Ni-foam with deposited material was soaked in distilled water for 20 min, rinsed several times with distilled water and ethanol, respectively, and finally dried in a conventional oven at 60°C for 12 h. This oven-dried sample is designated as Co_3O_4-uc. Similar procedure was adopted to synthesize cobalt oxide using 0.6 mmol of cetyltrimethylammonium bromide (CTAB) and 0.6 mmol of 4-octylphenol polyethoxylate (Triton X-100) surfactants and the corresponding oven-dried samples are named as Co_3O_4-C-uc and Co_3O_4-T-uc, respectively. In order to convert corresponding oxides, the as-grown precursor materials on Ni-foams were heated slowly from room temperature to 350°C at the heating rate of 1°C min^{-1} and kept at 350°C for 2 h by flowing air. These calcined samples are designated as Co_3O_4, Co_3O_4-C and Co_3O_4-T.

2.2 *Characterization*

In order to avoid the strong intense peaks of Ni-foam, cobalt oxide powder samples were collected from the Ni-foam and used for powder X-ray diffraction (PXRD). The PXRD patterns recorded from 10° to 80° using Bruker AXS D8 Advance diffractometer at room temperature employing Cu Kα ($\lambda = 0.15408$ nm) radiation generated at 40 kV and 30 mA. The crystallite size of all the Co_3O_4 samples was approximated by using the Debye-Scherrer equation; $D = K\lambda/(\beta\cos\theta)$, where D is the linear dimension of the particle (particle size), K is the spherical shape factor (0.89), and β is the full width at half-maximum height (fwhm) of the respective peaks measured graphically.

Multipoint N_2 adsorption-desorption experiment was carried out on an automatic Micromeritics ASAP 2020 analyzer and the surface area was determined using the Brunauer-Emmett-Teller (BET) gas adsorption method at 77 K. The cobalt oxide samples collected from Ni-foams were outgassed at 150°C for 12 h in dynamic vacuum before physisorption measurements. The pore size distribution plots were generated from desorption branch of the isotherm by the Barrett-Joyner-Halenda (BJH) method. The pore volume was obtained from the pore size distribution data. Surface morphologies of the calcined samples were obtained using an FEI Quanta FEG 400 high-resolution scanning electron microscope (HRSEM). The cobalt oxide deposited Ni-foams were placed on a conducting carbon tape before being mounted on the microscope sample holder for analysis. The high resolution transmission electron microscopy (HRTEM) studies were recorded on a JEOL 3010 HRTE microscope operated at 300 kV.

2.3 *Electrochemical measurements*

The supercapacitor performance of the Co_3O_4/Ni-foam materials was evaluated by cyclic voltammetry (CV), chronopotentiometry (CP) and electrochemical impedance spectroscopy (EIS) measurements. All these experiments have been carried out using conventional three-electrode configuration on a CHI 7081C electrochemical workstation. Ni-foams deposited with Co_3O_4 (~2–4 mg cm^{-2}, mass loading was evaluated from the difference in weight before and after deposition of the active material on Ni-foam) served as working electrodes while a square Pt foil (1 × 2 cm^2) and Hg/HgO (1.0 mol L^{-1} KOH) electrodes served as counter and reference electrodes, respectively. Freshly prepared aqueous KOH (2.0 M) electrolyte was used for supercapacitor study. The cobalt oxide electrodes were stabilised initially for 100 CV cycles before the final measurements.

3. Results and Discussion

3.1 *Characterization of Co_3O_4*

The powder X-ray diffraction (PXRD) patterns of all calcined samples Co_3O_4, Co_3O_4-C and Co_3O_4-T are shown in Figure 1. The formation of nano-crystalline face centered cubic Co_3O_4 phase is confirmed from the PXRD reflections indexed at 2θ values of 19.0° (111), 31.3° (220), 36.8° (311), 38.5° (222), 44.8° (400), 59.3° (511) and 65.2° (440). The average crystallite sizes, calculated from the major peaks of Co_3O_4, Co_3O_4-C and Co_3O_4-T materials using Debye-Scherrer equation, were in the nanoscale range (Table 1). The data shows that the surfactants are effective in producing smaller crystallite sizes due to selective interaction between surfactant molecules and metal precursors.

The surface morphologies of spinel cobalt oxide materials (Co_3O_4, Co_3O_4-C and Co_3O_4-T) grown on Ni-foam examined by HR-SEM are shown in Figure 2. The cationic (CTAB), non-ionic (TritonX-100) surfactant-assisted cobalt oxide materials (Co_3O_4-C, Co_3O_4-T) and surfactant-free synthesized Co_3O_4 material grown on Ni-foam are shown in Figures 2(a), 2(d) and 2(g), respectively. The insets of these figures show the bare Ni-foam (before deposition of cobalt oxide). Intriguingly, Co_3O_4-C (Figures 2b and 2c) and Co_3O_4-T (Figures 2e and 2f) materials show ultrathin nanoflake morphologies, and they differ only in flakes arrangements whereas Co_3O_4 (Figures 2h and 2i) exhibits flower-like morphology. In the case of Co_3O_4-C material, ultrathin nanoflakes are arranged in a regular fashion and perpendicularly projected with larger gaps while randomly oriented nanoflakes are seen in Co_3O_4-T.

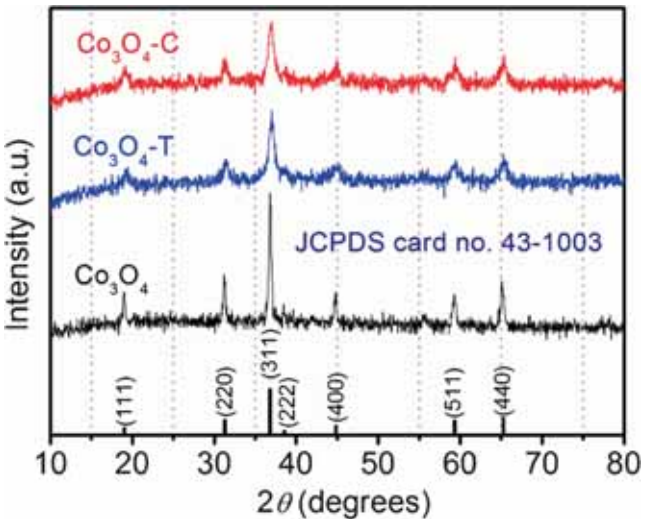

Figure 1. PXRD patterns of Co_3O_4, Co_3O_4-C and Co_3O_4-T materials grown *in situ* on Ni-foam and collected for phase analysis.

The reason for this is hydrophilic part of the cationic CTAB molecule can adsorb counter anions and the hydrophobic part of the molecules can come close together leading to the large separation of nanoflakes in the final growth of Co_3O_4-C shown in Figure 3. In Triton X-100 assisted synthesis, the growth of Co_3O_4 precursors occurred on the chains of Triton X-100 leading to the formation of closely aggregated nanoflakes. While without surfactant, the growth of Co_3O_4 precursor takes flower-like shape (Figure 3). However, the growth of different nanostructures with distinct morphologies and diverse crystal facets during the synthesis is at present elusive but can depend on the number of factors which include electrostatic interactions, hydrophobic interactions, van der Waals forces, hydrogen bonding and crystal face attraction.[2,3,11,32–34] Generally, inorganic and organic moieties, nature of precipitating agent and solvent, reaction temperature

Table 1. The physicochemical properties and specific capacitance values at a current density of 1 A g^{-1} of Co_3O_4, Co_3O_4-C and Co_3O_4-T materials on Ni-foam in comparison with bare Ni-foam. The cobalt oxide powders were collected separately from Ni-foam for physicochemical analysis. Cobalt oxide on Ni-foam samples were directly used for specific capacitance measurements.

Sample	Average crystallite size (nm)	Morphology	Specific surface area (m^2g^{-1})	Pore volume (cm^3g^{-1})	Pore diameter (nm)	Specific capacitance (F g^{-1})
$Co_3O_4^*$	26	Flower	27	0.10	10	288
Co_3O_4-C[#]	9.8	Nanoflakes	66	0.16	3.8	1820
Co_3O_4-T[§]	6.6	Nanoflakes	80	0.17	3.8	806
Ni-foam[†]	–	Porous	~4	~0.015	~9	~20

*Sample synthesized on Ni-foam without using surfactant; [#]sample synthesized on Ni-foam using CTAB; [§]sample synthesized on Ni-foam using Triton X-100; [†]Bare Ni-foam which is largely macroporous, number of pores per inch 80–120, density 0.35–0.67 g cm^{-3}, porosity ≥95%; thickness 1.2 mm, (Courtesy: CSIR CECRI-Madras Unit, Taramani).

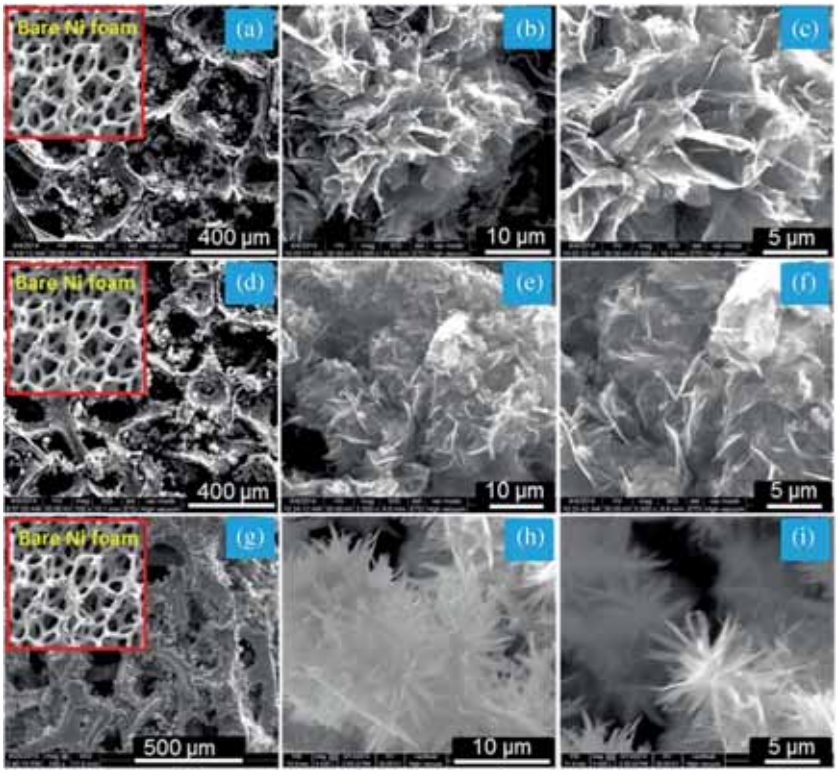

Figure 2. HR-SEM images of Co_3O_4-C (a–c), Co_3O_4-T (d–f) and Co_3O_4 (g–i) grown on Ni-foam.

and time are all factors which influence the final morphology of oxide materials.[2,3,11–14,26–29,32–37] In our work, the change in morphology is mainly due to the presence of surfactant molecules since other synthesis conditions are same in all cases. It is pointed out in the literature that the specific adsorption of surfactant molecules (CTAB and Triton X-100) on a selective crystal-facet undergoes kinetic shape control, and causes the formation flake-like structure.[2] The low and high magnification HR-TEM images of all three cobalt oxide materials are shown in Figure 4. The lattice fringes are also clearly seen in the insets. The lattice fringes of Co_3O_4-C sample have an averaged d spacing of 0.24 nm and 0.283 nm corresponding to the (311) and (220) set of planes, respectively (inset of Figure 4b). In the case of Co_3O_4-T and Co_3O_4 samples, the averaged d spacing is 0.283 nm which corresponds to the (220) plane (inset of Figures 4d and 4f). These results are in accordance with the PXRD results of Co_3O_4.

Figure 5a shows N_2 adsorption-desorption isotherms of Co_3O_4, Co_3O_4-C and Co_3O_4-T materials which resemble type-IV isotherms with H1 hysteresis loop.[11,28,38] This clearly indicates that all the materials contain mesopores. The existence of mesoporosity in these samples is also confirmed from the BJH measurements shown in Figure 5b. The specific surface area,

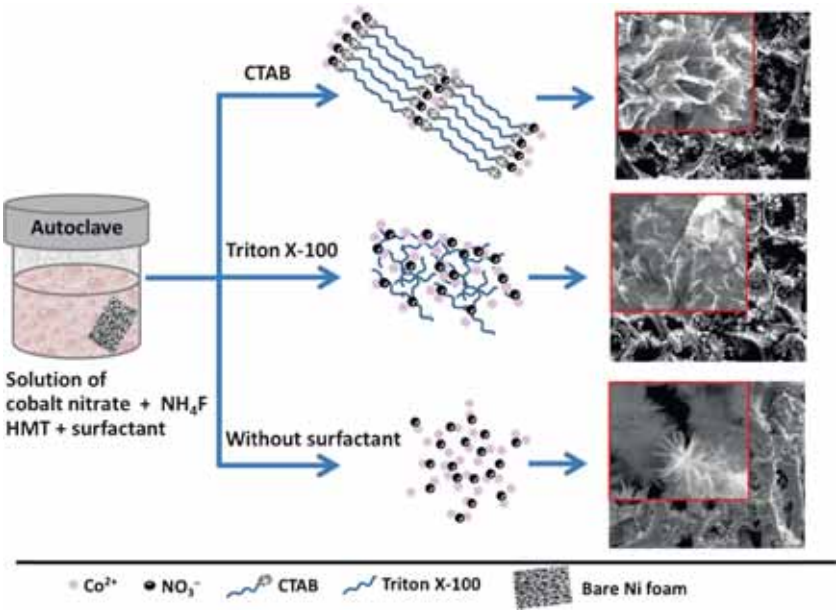

Figure 3. Schematic illustration for the formation of nanoflake and flower-like morphologies of nanostructured cobalt oxide material with and without using surfactants.

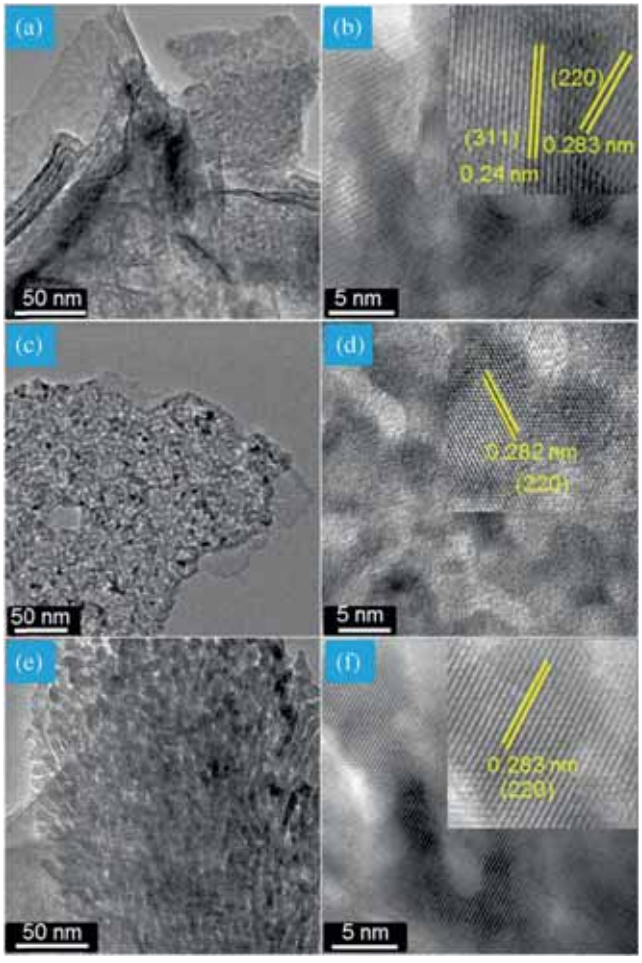

Figure 4. HR-TEM images of Co_3O_4-C (a and b) and Co_3O_4-T (c and d) synthesized by using surfactants, Co_3O_4 (e and f) synthesized without surfactant.

pore volume and pore diameter of Co_3O_4-C, Co_3O_4-T and Co_3O_4 materials have been obtained, respectively, from BET and BJH pore size distribution analysis which are shown in Table 1. The average pore size in Co_3O_4-C and Co_3O_4-T materials is ~3.8 nm which is better suited for supercapacitor applications. This type of pore size distribution is commonly observed in materials synthesized using surfactant templates.[26,28] The results show that the specific surface area and pore volume are much higher for Co_3O_4-C and Co_3O_4-T materials compared to Co_3O_4 material (Table 1).

3.2 *Capacitive performance of Co_3O_4 materials*

Due to the differences in morphology, crystallite size, surface area and porosity of Co_3O_4, Co_3O_4-C and Co_3O_4-T materials, the electrochemical properties of these materials are expected to be different. The high surface area and mesoporous nanoflakes composed of smaller nanocrystallites of Co_3O_4-C and Co_3O_4-T materials provides more number of active sites for electrolyte ions for more redox reactions. The comparison of charge storage efficiencies of Co_3O_4, Co_3O_4-C and Co_3O_4-T materials grown on Ni-foam were studied by CV, CP and EIS measurements in aqueous KOH (2 M) electrolyte. Figure 6a shows the CV profiles of three cobalt oxide electrode materials recorded at a scan rate of 10 mV s^{-1}. The resultant redox peaks in CV curves are due to $Co_3O_4/CoOOH/CoO_2$ transformations during the interaction of OH^- ions with the cobalt oxide electrodes.[10–14,39] However, the CV

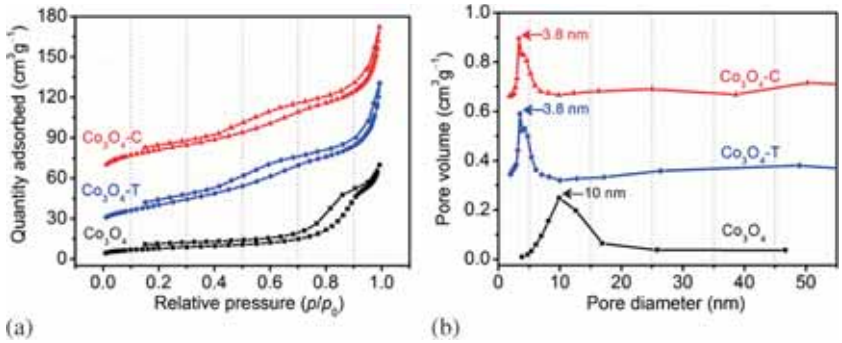

Figure 5. (a) BET isotherms and (b) BJH pore size distribution profiles of Co_3O_4, Co_3O_4-C and Co_3O_4-T materials. For these analyses, oxide powders were collected from the Ni-foam

pattern of Co_3O_4 strongly depends on its morphology and surface properties. In the present study, the peaks corresponding to Co(II)↔Co(III)↔Co(IV) are not distinguishable due to low crystallinity and other microstructural effects of the sample.[10–17] The Co_3O_4-C and Co_3O_4-T electrodes showed higher oxidation and reduction peak currents compared to Co_3O_4 electrode (Co_3O_4-C>Co_3O_4-T>Co_3O_4). This result is attributed to smaller crystallite sizes, larger surface areas and favourable mesoporous nanoflake morphologies of Co_3O_4-C and Co_3O_4-T materials. These features are advantageous for easy transportation of electrolyte ions into the accessible redox cobalt oxide matrix. The redox reactions are more feasible and efficient in Co_3O_4-C and Co_3O_4-T electrode materials leading to higher current density. Between these two materials, nanoflakes of Co_3O_4-C material provides additional electroactive sites due to availability of free space among the nanoflakes, therefore this material has highest peak current compared to the nanoflakes of Co_3O_4-T. In order to know the contribution of Ni-foam, we recorded CV of bare Ni-foam and compared with the CVs of cobalt oxide materials as shown in Figure 6a. The insignificant peak current of bare Ni-foam signifies that the oxide material deposited on Ni-foam is solely responsible for higher redox peak current. The very

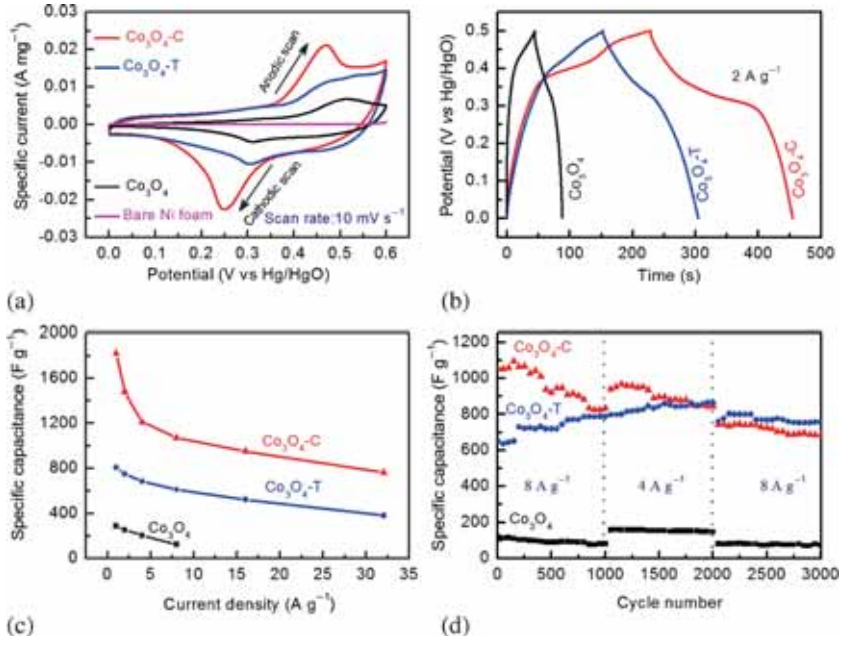

Figure 6. Electrochemical behaviour of Co_3O_4, Co_3O_4-C and Co_3O_4-T electrode materials grown on Ni-foam. (a) Cyclic voltammograms at 10 mV s^{-1} scan rate; (b) Galvanostatic charge-discharge cycles at current density of 2 A g^{-1}; (c) Comparison of specific capacitance values at different current densities; (d) Cyclic stability at current densities of 4 and 8 A g^{-1}.

low specific surface area and porosity of the bare Ni-foam compared to Co_3O_4/Ni-foam (Table 1) also tells the insignificant contribution of Ni-foam to the total capacitance. The differences in the redox peak currents and peak potentials of the three oxide electrode materials are due to difference in their surface morphologies, crystallite sizes and spatial arrangements in nanoflakes. In Co_3O_4-C material, the nanoflakes are perpendicularly projected with larger gaps (Figure 2c). Hence, the electrolyte can easily pass through these gaps which causes more number of cobalt oxide sites to be involved in the Faradaic processes efficiently.

The galvanostatic charge-discharge cycles recorded at a current density of 2 A g^{-1} are shown in Figure 6b. Here, both Co_3O_4-C and Co_3O_4-T electrodes show sluggish potential drop in the discharge curves compared to Co_3O_4 electrode at a fixed current density. This behaviour demonstrates that both Co_3O_4-C and Co_3O_4-T electrode materials are excellent for energy storage and delivery. These three electrodes have been tested at different current densities and their specific capacitance values (C_S, F g^{-1}) are calculated using equation 1, and the corresponding discharge curves are shown in Figure S1a-c (in Supplementary Information).

$$C_s = \frac{i}{m\,(\Delta V/\Delta t)} \tag{1}$$

Where i is the discharging current (A), m is the mass of material (g), ΔV is the operating potential (V) and Δt is the discharging time (s).

In Figure 6c, the variation of specific capacitance with current density is compared for the three electrodes. Among the three, Co_3O_4-C exhibits highest C_S values of 1820 F g^{-1} at 1 A g^{-1}, and 1070 F g^{-1} at 8 A g^{-1}. At same current densities, the C_S values for Co_3O_4-T and Co_3O_4 were found to be 806 and 611, and 288 and 126 F g^{-1}, respectively. The higher C_S values for Co_3O_4-C and Co_3O_4-T electrodes are attributed primarily to smaller crystallite sizes, higher surface area as well as higher pore volume of nanoflake morphologies. These unique features have been shown to be favourable for transportation and diffusion of electrolyte ions during the charge-discharge processes. In Co_3O_4-C case, the inner and outer surfaces are efficiently accessed by the electrolyte ions due to the existence of larger gap between the nanoflakes and this leads to high C_S compared to Co_3O_4-T. The C_S values obtained for nanoflakes of Co_3O_4-C and Co_3O_4-T are quite high compared to the recently reported values which are given in Table S1 (in Supplementary Information). Yuan *et al.*, obtained very high C_S value of 2735 F g^{-1} at 2 A g^{-1} by electrochemical deposition method, but large scale synthesis of material may not be negotiable.[15] Yang *et al.*, used two-step hydrothermal approach to achieve high specific capacitance value of 1782 F g^{-1} at 1.8 A g^{-1}.[12] In the present study, we have obtained high C_S value of 1820 F g^{-1} at 1 A g^{-1} employing simple single step hydrothermal method, which is suitable to synthesize the material in large scale. Since the retention of capacitance for longer period of charge-discharge cycles is an essential criterion for practical applications, we have tested the stability of the three electrodes by carrying out 3000 charge-discharge cycles at current densities of 8 and 4 A g^{-1}. Initially 1000 cycles were recorded at 8 A g^{-1} followed by 1000 cycles at 4 A g^{-1}, and finally 1000 cycles were recorded at 8 A g^{-1}. The specific capacitance values calculated at every 50th cycle using equation 1 are plotted in Figure 6d. The specific capacitance retention values of the three electrodes are also presented in Table S2 (in Supplementary Information).

It is evident from Figure 6d and Table S2 (in Supplementary Information) that the specific capacitance decay is observed only for Co_3O_4 and Co_3O_4-C electrode materials. However, Co_3O_4-C electrode material shows only 8% C_S loss in the last 1000 cycles. There seems to be some structural deactivation by means of restacking of the nanoflakes which is responsible for the initial C_S loss during charge-discharge cycles (up to 2000 cycles). In the case of Co_3O_4-T electrode, interestingly and impressively, the specific capacitance value increased up to 2000 cycles. The enhancement in specific capacitance is attributed to structural activation of Co_3O_4-T which happens due to the separation of the stacked cobalt oxide nanoflakes. The structural activation in turn translates to pore opening and increase in electroactive surface area of Co_3O_4-T material.[14,27,28] The capacitance retention of Co_3O_4-C and Co_3O_4-T electrodes is much higher compared to the recent reports cited in Table S1 (in Supplementary Information). The exceptionally high C_S values (Figure 6c) and capacitance retention of Co_3O_4-C and Co_3O_4-T electrode materials (Figure 6d and Table S2) are due to low solution resistance (R_s), charge transfer resistance (R_{ct}) and Warburg impedance (Z_w) depicted in Figure 7. In this Nyquist plot, the intersection of semi-circle at the real axis in the high frequency region represents the $R_{s,}$ the diameter of semicircle represents the R_{ct} and the inclined straight line in the low frequency region shows the Z_w (Figure 7).[26–29,39,40] The Co_3O_4-C and Co_3O_4-T samples do not exhibit significant semi-circle indicating very low R_{ct} between the active material/electrolyte interface.[39] The Co_3O_4-C sample exhibits less R_s compared to Co_3O_4-T. The linear portions of the

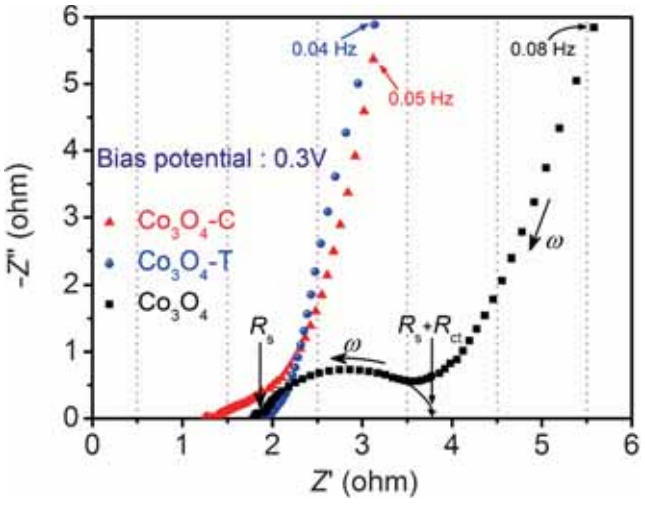

Figure 7. Nyquist plots of Co_3O_4, Co_3O_4-C and Co_3O_4-T electrode materials on Ni-foam recorded at 0.3 V bias potential.

Nyquist plots of Co_3O_4-C and Co_3O_4-T electrodes tend to be nearly parallel to the imaginary axis which is a characteristic feature of good capacitive behaviour.[8,10,11,26–29,39] In general, low time constant (τ) is preferred for fast charge-discharge electrode characteristics. The value of τ for all cobalt oxide materials is calculated using equation $\tau = 1/2\pi f^*$, where f^* denotes the frequency corresponding to maximum of the imaginary component ($-Z''$).[27,29] The estimated τ values for Co_3O_4-C, Co_3O_4-T and Co_3O_4 are 0.3, 19.7 and 111 ms, respectively. The porous flake-like morphology reduces the transportation/diffusion time for electrons and ions. Hence, high C_S values of Co_3O_4-C and outstanding capacity retention of Co_3O_4-T electrode materials are expected due to fast electrode kinetics promoted by easy access of electrolyte/electrode interface to the electrolyte ions.

Broadly, the excellent supercapacitor performance of the nanoflakes of cobalt oxide electrodes can be attributed to multiple factors. These factors include smaller crystallite size, numerous inter-connected pores on cobalt oxide nanoflakes which result in large surface area and intimate contact between the nanoflakes and surface of the Ni-foam. This facilitates the transport of electrolyte ions and electrons which give rise to low values of R_s, R_{ct}, Z_w and τ.

4. Conclusions

The electrochemical properties of an electrode material strongly depend on the morphology, particle size, porosity and surface area of oxide material. These aspects are demonstrated in this work by systematically comparing the physicochemical and electrochemical properties of cobalt oxide samples synthesized as surfactant-free (Co_3O_4), CTAB-assisted (Co_3O_4-C) and Triton X-100-assisted (Co_3O_4-T). The surfactants have shown significant impact on particle size, morphology, porosity and surface area. Among all the three electrode materials, Co_3O_4-C exhibited very high C_S value (1820 F g^{-1} at 1 A g^{-1}). The Co_3O_4-T electrode exhibited excellent capacitance retention and there was substantial enhancement in C_S during the charge-discharge cycles. The nanoflake morphologies and porous structures of Co_3O_4-C and Co_3O_4-T materials provide more active sites, and efficient contact between the electrode and electrolyte ions. These are favourable attributes of nanostructured cobalt oxide for better performance towards charge storage. The significant differences in the specific capacitance values and stabilities of both Co_3O_4-C and Co_3O_4-T materials are primarily attributed to the differences in packing of nanoflakes.

Supporting information (SI)

The comparison of specific capacitance values and capacity retention of recent reports (Table S1), the comparison of specific capacitance retention values (Table S2) and galvanostatic discharge profiles of Co_3O_4-C, Co_3O_4-T and Co_3O_4 materials (Figures S1a to S1c) are given in the supporting information, available at www.ias.ac.in/chemsci.

Acknowledgements

GR and EU would like to thank the UGC and CSIR, New Delhi for granting the JRF and SRF fellowships, respectively. Authors thank the DST, New Delhi, for FIST experimental facilities and MNRE (102/28/2006-NT) for funding.

References

1. Shukla A K, Sampath S and Vijayamohanan K 2000 Electrochemical supercapacitors: Energy storage beyond batteries *Current Sci.* **79** 1656
2. Sun H, Ang H M, Tadé M O and Wang S 2013 Co_3O_4 nanocrystals with predominantly exposed facets: Synthesis, environmental and energy applications *J. Mater. Chem. A* **1** 14427
3. Patzke G R, Zhou Y, Kontic R and Conrad F 2011 Oxide nanomaterials: Synthetic developments, mechanistic studies, and technological innovations *Angew. Chem. Int. Ed.* **50** 826
4. Xia X, Zhang Y, Chao D, Guan C, Zhang Y, Li L, Ge X, Bacho I M, Tu J and Fan H J 2014 Solution synthesis of metal oxides for electrochemical energy storage applications *Nanoscale* **6** 5008
5. Meher S K and Ranga Rao G 2014 Novel nanostructured CeO_2 as efficient catalyst for energy and environmental applications *J. Chem. Sci.* **126** 361

6. Vivekchand S R C, Rout C S, Subrahmanyam K S, Govindaraj A and Rao C N R 2008 Graphene-based electrochemical supercapacitors *J. Chem. Sci.* **120** 9
7. Devaraj S, Gabriel G S, Gajjela S R and Balaya P 2012 Mesoporous MnO_2 and its capacitive behaviour *Electrochem. Solid State Lett.* **15A** 57
8. Umeshbabu E, Rajeshkhanna G and Ranga Rao G 2016 Effect of solvents on the morphology of $NiCo_2O_4$/graphene nanostructures for electrochemical pseudocapacitor application *J. Solid State Electrochem.* **20** 1837
9. Umeshbabu E, Rajeshkhanna G, Justin P and Ranga Rao G 2016 $NiCo_2O_4$/rGO hybrid nanostructures for efficient electrocatalytic oxygen evolution *J. Solid State Electrochem. J. Solid State Electrochem.* **20** 2725
10. Meher S K and Ranga Rao G 2011 Effect of microwave on the nanowire morphology, optical, magnetic, and pseudocapacitance behavior of Co_3O_4 *J. Phys. Chem. C* **115** 25543
11. Meher S K and Ranga Rao G 2011 Ultralayered Co_3O_4 for high-performance supercapacitor applications *J. Phys. Chem. C* **115** 15646
12. Yang Q, Lu Z, Sun X and Liu J 2013 Ultrathin Co_3O_4 nanosheet arrays with high supercapacitive performance *Sci. Rep.* **3** 3537
13. Wang X, Yao S, Wu X, Shi Z, Sun H and Que R 2015 High gas-sensor and supercapacitor performance of porous Co_3O_4 ultrathin nanosheets *RSC Adv.* **5** 17938
14. Zhang X, Zhao Y and Xu C 2014 Surfactant dependent self-organization of Co_3O_4 nanowires on Ni foam for high performance supercapacitors: From nanowire microspheres to nanowire paddy fields *Nanoscale* **6** 3638
15. Yuan C, Yang L, Hou L, Shen L, Zhang X and Lou X W 2012 Growth of ultrathin mesoporous Co_3O_4nanosheet arrays on Ni foam for high-performance electrochemical capacitors *Energy Environ. Sci.* **5** 7883
16. Shim H-W, Lim A-H, Kim J-C, Jang E, Seo S-D, Lee G-H, Kim T D and Kim D-W 2013 Scalable one-pot bacteria-templating synthesis route toward hierarchical, porous-Co_3O_4 superstructures for supercapacitorelectrodes *Sci. Rep.* **3** 2325
17. Dong X-C, Xu H, Wang X-W, Huang Y-X, Chan-Park M B, Zhang H, Wang L-H, Huang W and Chen P 2012 3D grapheme cobalt oxide electrode for high-performance supercapacitor and enzymeless glucose detection *ACS Nano* **6** 3206
18. Dinga Y, Wanga Y, Sua L, Bellagambaa M, Zhangb H and Lei Y 2010 Electrospun Co_3O_4nanofibers for sensitive and selective glucose detection *Biosens. Bioelectron.* **26** 542
19. Jena A, Munichandraiah N and Shivashankar S A 2015 Metal-organic chemical vapor-deposited cobalt oxide films as negative electrodes for thin film Li-ion battery *J. Power Sources* **277** 198
20. Rajeshkhanna G, Umeshbabu E and Ranga Rao G 2017 Charge storage, electrocatalytic and sensing activities of nest-like nanostructured Co_3O_4 *J. Colloid Interface Sci.* **487** 20
21. Xia H, Peng Z, Cuncal L V, Zhao Y, Hao J and Huang Z 2016 Self-supported porous cobalt oxide nanowires with enhanced electrocatalytic performance toward oxygen evolution reaction *J. Chem. Sci.* doi:10.1007/s12039-016-1192-z
22. Li X, Fang Y, Lin X, Tian M, An X, Fu Y, Li R, Jin J and Ma J 2015 MOF derived Co_3O_4 nanoparticles embedded in N-doped mesoporous carbon layer/MWCNT hybrids: Extraordinary bi-functional electrocatalysts for OER and ORR *J. Mater. Chem. A* **3** 17392
23. Song H, Shen L and Wang C 2014 Template-free method towards quadrate Co_3O_4nanoboxes from cobalt coordination polymer nano-solids for high performance lithium ion battery anodes *J. Mater. Chem. A* **2** 20597
24. Simon P and Gogotsi Y 2008 Materials for electrochemical capacitors *Nat. Mater.* **7** 845
25. Vijayanand S, Kannan R, Potdar H S, Pillai V K and Joy P A 2013 Porous Co_3O_4 nanorods as superior electrode material for supercapacitors and rechargeable Li-ion batteries *J. Appl. Electrochem.* **43** 995
26. Umeshbabu E, Rajeshkhanna G and Ranga Rao G 2014 Urchin and sheaf-like $NiCo_2O_4$nanostructures: Synthesis and electrochemical energy storage application *Int. J. Hydrogen Energy* **39** 15627
27. Syedvali P, Rajeshkhanna G, Umeshbabu E, Kiran G U, Ranga Rao G and Justin P 2015 *In situ* fabrication of graphene decorated microstructured globe artichokes of partial molar nickel cobaltite anchored on a Ni foam as a high performance supercapacitor electrode *RSC Adv.* **5** 38407
28. Rajeshkhanna G, Umeshbabu E, Justin P and Ranga Rao G 2015 *In situ* fabrication of porous festucascoparia-like $Ni_{0.3}Co_{2.7}O_4$ nanostructures on Ni-foam: An efficient electrode material for supercapacitor applications *Int. J. Hydrogen Energy* **40** 12303
29. Umeshbabu E, Rajeshkhanna G, Justin P and Ranga Rao G 2015 Synthesis of mesoporous $NiCo_2O_4$-rGO by solvothermal method for charge storage applications *RSC Adv.* **5** 66657
30. Zhang Q, Deng Y, Hu Z, Liu Y, Yao M and Liu P 2014 Sea urchin-like hierarchical $NiCo_2O_4$@$NiMoO_4$ core-shell nanomaterials for high performance supercapacitors *Phys. Chem. Chem. Phys.* **16** 23451
31. Cheng G, Yang W, Dong C, Kou T, Bai Q, Wang H and Zhang Z 2015 Ultrathin mesoporous NiO nanosheet-anchored 3D nickel foam as an advanced electrode for supercapacitors *J. Mater. Chem. A* **3** 17469
32. Hu L, Peng Q and Li Y 2008 Selective synthesis of Co_3O_4nanocrystal with different shape and crystal plane effect on catalytic property for methane combustion *J. Am. Chem. Soc.* **130** 16136
33. Dam D T and Lee J-M 2014 Three-dimensional cobalt oxide microstructures with brush-like morphology *via* surfactant-dependent assembly *ACS Appl. Mater. Interfaces* **6** 20729
34. Whitesides G M and Boncheva M 2002 Beyond molecules: Self-assembly of mesoscopic and macroscopic components *Proc. Natl. Acad. Sci.* **99** 4769
35. Xia X-H, Tu J-P, Wang X-L, Gu C-D and Zhao X-B 2011 Mesoporous Co_3O_4 monolayer hollow-sphere array as electrochemical pseudocapacitor material *Chem. Commun.* **47** 5786
36. Liu Z-Q, Xiao K, Xu Q-Z, Li N, Su Y-Z, Wang H-J and Chen S 2013 Fabrication of hierarchical flower-like super-structures consisting of porous $NiCo_2O_4$ nanosheets and their electrochemical and magnetic properties *RSC Adv.* **3** 4372

37. Mei W, Huang J, Zhu L, Ye Z, Mai Y and Tu J 2012 Synthesis of porous rhombus-shaped Co_3O_4nanorod arrays grown directly on a nickel substrate with high electrochemical performance *J. Mater. Chem.* **22** 9315
38. Rouquerol F H, Rouquerol J and Sing K 1999 In *Adsorption by powders and porous solids* (London: Academic Press)
39. Wang X, Sumboja A, Khoo E, Yan C and Lee P S 2012 Cryogelsynthesis of hierarchical interconnected macro-/mesoporous Co_3O_4 with superb electrochemical energy storage *J. Phys. Chem. C* **116** 4930
40. Xia Q X, Hui K S, Hui K N, Kim S D, Lim J H, Choi S Y, Zhang L J, Mane R S, Yun J M and Kim K H 2015 Facile synthesis of manganese carbonate quantum dots/Ni$(HCO_3)_2$-$MnCO_3$ composites as advanced cathode materials for high energy density asymmetric supercapacitors *J. Mater. Chem. A* **3** 22102